Keywords

Apatite-forming ability, Bioactivity, Surface mineralization, Ca/P ratio, Surface chemical reactivity, Dental cement.

Author

Dr. njwan shehab *
*Department of Conservative Dentistry/ College of Dentistry/University of Mosul/ Mosul/ Iraq
njwanshehab2@gmail.com
njwandent@uomosul.edu.iq

Received: 13.01.2026
Accepted: 23.01.2026
Doi: 10.1922/ejprd.v34i2.1420

Bone substitute nanomaterials for enhancing the apatite-forming capacity of dental repair material

ABSTRACT

***Objective*:** To analyse the apatite-forming ability of mineral trioxide aggregate (MTA Angelus) modified with nano-carbonated hydroxyapatite (nCHAp) as a bioactive endodontic biomaterial.

Methods*:** Disc specimens (10.0 ± 0.1 mm diameter; 2.0 ± 0.1 mm thickness) were made-up from unmodified MTA (control) and MTA hold 2, 3, and 4 wt% nCHAp (n=12/group). After setting for 24 h at 37 °C and relative humidity, six specimens per group were immersed in 20 mL sterile phosphate-buffered saline (PBS, pH 7.4) at 37 °C for 21 days with PBS renewal every 3 days; the remaining six were stored dry. Surface mineralization was measured by field-emission scanning electron microscopy (FESEM), energy-dispersive X-ray spectroscopy (EDX; five spots/specimen) with Ca/P ratio calculation, and X-ray diffraction (XRD) for phase finding. Statistical analysis was performed using ANOVA/Tukey tests ($\alpha = 0.05$). ***Results: PBS exposure evoked calcium-phosphate deposition on all immersed specimens. Unmodified MTA showed porous spherical Ca–P aggregates agreeable with amorphous calcium phosphate; phosphorus emerged (13.60 wt%) and Ca/P was 2.49, indicating calcium-rich, immature surface deposits. Adding nCHAp boosted mineralization, and the effect got stronger with higher concentrations. At 2 wt%, it created an early layer with a change into flat, plate-like crystals. When the concentration went up to 3–4 wt%, it formed continuous nano-sized apatite layers with needle and plate shapes, along with rosette-like clusters. After soaking, the calcium-to-phosphorus ratios dropped a bit—down to around 1.80 for 2%, 1.76 for 3%, and 1.70 for 4%—getting closer to normally seen in natural bone. XRD results showed clear signs of hydroxyapatite/carbonated hydroxyapatite reflections with decreased silicate/portlandite intensities after immersion. Conclusions: Adding 2–4 wt% nCHAp speeds up the natural-like apatite formation on MTA, boosting its chances for regenerative endodontic repair and strengthening the mineral layer where dentin meets the material.

Clinical Relevance: Improving the bioactivity helps the seal become stronger and supports the hard tissue in healing better. This could make MTA last longer and perform more reliably during root canal treatments.

INTRODUCTION

In recent years, there's been some exciting advancement in dental materials. New fillings and products that help regrow bone. These advances are shifting how dentists treat patients and making outcomes better[1]. These days, there's a focus on bioactive material because they interact with biological tissues when they touch cells. They aid natural repair and regeneration processes, which ultimately lead to better oral health[2]. Calcium hydroxide, the first endodontic material known for its ability to encourage the formation of a dentinal bridge over exposed pulp tissue[3]. Over time, newer materials like mineral trioxide aggregate (MTA) and similar calcium silicate cements were developed. These are basically portland cement mixed with bismuth oxide to make them visible on X-rays. These hydraulic bioceramics have become popular for use in procedures like vital pulp therapy, repairing perforations, and other dental repairs[4]. Their bioactivity comes from releasing calcium ions, which react with phosphate in the body fluids, this creates hydroxyapatite crystals on the surface of the material to support tissue repair[5].

Bioactivity refers to ability of dental materials to interact with tissues and help tissues to heal by encouraging the formation of apatite at the material–tissue interface. This feature is useful in endodontic applications[6]. Mineral Trioxide Aggregate (MTA) is a calcium silicate-based cement used in root treatments, known for its good biological properties. But its bioactivity has some issues. For instance, forming an apatite layer on MTA slow and uneven process, which might impact the material to seal properly and support the remineralization of dentin[7]. Its ability to interact biologically comes from releasing calcium and hydroxyl ions. These ions then react with phosphate in the nearby fluids, forming a calcium-phosphate layer on the surface. This layer helps the material bond better with dental tissues[8]. However, since MTA doesn't have phosphate inside itself, it depends on phosphate from outside sources. That means it takes longer for it to start forming apatite compared to materials that include phosphate-releasing components right in their structure[9, 10]. Researchers are constantly working to make MTA better by boosting its ability to interact with tissues. One exciting idea is to bone-like materials, like nano carbonate-substituted hydroxyapatite (nCHA), it is similar to the minerals in bones and teeth. Research shows that nCHA helps formation of more organized and quicker-growing apatite crystals, ultimately improving bioactivity of materials and clinical performance[11]. Thus, incorporating nCHA into MTA could provide extra nucleation sites, accelerate calcium-phosphate deposition, and enhance mineral induction.

MATERIAL AND METHODS

Bioactivity assessment

The bioactivity of the cement formulations was checked using the ISO 23317:2014 [12] standards, testing how implant materials can form apatite in vitro. Chiefly, if a material can grow a clear layer of apatite on its surface within 21 days while soaked in a simulated body fluid, it's realized as bioactive. In this study, PBS was used as the soaking solution.

Specimen preparation and immersion protocol

Disc-shaped specimens about (2.0 ± 0.1) mm in thick and (10.0 ± 0.1) mm in diameter were prepared for both control and experimental groups. Cements were mixed per the manufacturers' instructions and placed into plastic molds on polyethylene-lined glass slabs to prevent adhesion. A second polyethylene-covered glass slab was applied to ensure surface uniformity by removing excess material. Thus, the resulting specimens with smooth flat surfaces. The specimens were then incubated at 37 °C with 95% relative humidity for 24 hours to simulate intraoral conditions and allow complete setting. Following setting, specimens were demolded, and surface irregularities were refined using fine abrasive paper. Twelve specimens (n = 12 per group) for each of the Angelus MTA (Angelus, Londrina, PR, Brazil) without nanoparticles (control positive) and the MTA with 2, 3, and 4% by weight of nCHA (99.9% purity; ~70 nm), supplied by Nano Research Elements Company (India), (experimental groups) were prepared. Six specimens per group were immersed in 20 mL of sterile PBS in screw-capped containers and incubated at 37 °C for 21 days to mimic long-term physiological exposure. The remaining six specimens were stored dry as negative controls.

Groups:

1. Control positive group (n=12): Angelus MTA without nanoparticles (before and after immersion). Six specimens per group were immersed and the remaining six specimens were stored dry.
2. Experimental groups: MTA with 2, 3, and 4% wt nCHA (before and after immersion), for each concentration (n=12). Six specimens per group were immersed. The remaining six specimens were stored dry as negative controls.

PBS was prepared by dissolving 8.58 g of PBS powder (pH 7.4) in 1000 ml of distilled water under continuous stirring until completely dissolved.

The pH was adjusted to 7.4 and the solution was sterilized by autoclaving at 121 °C and 15 psi for 15 minutes, according to manufacturer's guidelines. To simulate renewal physiological fluids in vivo, PBS was replenished every 3 days during the immersion period[13]. PBS act as a physiological storage solution without calcium (Ca^{2+}) and magnesium (Mg^{2+}) ions. Its ionic makeup included: Sodium chloride (NaCl, 7.650 g/L), Disodium hydrogen phosphate (Na_2HPO_4 ,0.724), and Dipotassium hydrogen phosphate ($K2HPO_4$, 0.210), with the pH maintained at 7.4 at 25°C.

Post-Incubation Treatment and Analytical Procedures

After the 21-day of immersion, the specimens were retrieved out of the PBS and placed in a desiccator with phosphorus pentoxide (P_2O_5) at 37 °C for 24 hours to ensure they were completely dry. The specimen surfaces were subsequently examined for apatite formation using field-emission scanning electron microscopy (FESEM) (TESCAN MIRA3 France) for surface morphology of the specimens combined with Energy-Dispersive X-ray Spectroscopy (EDX) for elemental analysis, then Ca/P ratio was assessed, while X-ray diffraction (XRD) used to detect structural phase changes.

Evaluation of apatite-forming ability

The apatite-forming ability was evaluated by analyzing surface morphology and microstructural features before and after PBS immersion using (FESEM) combined with (EDX) for elemental analysis. EFSEM imaging was performed at 15 kV accelerating voltage and ~10 mA beam current, with micrographs captured at magnifications ranging from 10.0× to 25.0×, and up to 100× to visualize apatite-like surface deposits. EDX analysis quantified the weight percentages of chemical elements and to rank the surface calcium (Ca) / phosphorus (P) ratio as an indicator of apatite-phase formation. Both PBS- immersed and non-immersed specimens were analyzed to detect chemical composition alterations and to detect the bioactivity-induced morphological and chemical changes. The

samples were analyzed for each group, and five analysis spots were examined for each sample surface. The results were the averages of the data calculated[14]. Additionally, phase identification and crystallinity were assessed via (XRD) using Cu Kα radiation (λ = 1.5406 Å), operating at 30 kV and 30 mA, with a 2θ scanning range of 10°–80°, a step size of 0.02°, and 0.5 s per step. The hydroxyapatite (HAp) phase was identified using the International Center for Diffraction Data (ICDD) database: $Ca_{10}(PO_4)_6(OH)_2$ [ICDD 00-009-432][15].

RESULTS

Field emission scanning electron microscope analysis

The FESEM images at various magnifications showed clear differences in the surface textures between the control and experimental samples, both before and after soaking in PBS, Figure 1. The cement surface of MTA after 21 days in PBS coated with a continuous layer of calcium-phosphate deposits, composed mainly of highly porous spherical aggregates with a nano sponge like architecture. This morphology is typical of amorphous calcium phosphate (ACP). Plate-like crystallites consistent with octacalcium phosphate (OCP), a transitional phase that appears during the early stages of calcium-phosphate maturation.

MTA with 2% nCHA showed a noticeable mineral layer after soaking. The surface displayed rounded calcium-phosphate deposits that act as the initial mineral growth. A porous network of thin lamellar structures, suggesting that the initial amorphous calcium-phosphate was beginning to change into OCP. The stacked crystalline structures on the surface are a typical of carbonated hydroxyapatite. These features show that adding nCHA enhances and speed up the formation of apatite on MTA when exposed to phosphate-rich environments. Modified MTA with 3% nCHA revealed a noticeable progression of calcium-phosphate deposits across the surface. The surface became completely covered by a tightly packed layer of nano-crystalline with needle-like and short plate morphologies, which is typical as the apatite matures. While modified MTA with 4% nCHA revealed a continuous, apatite layer composed of needle- and plate-like crystallites arranged in rosette-like aggregates. It's clear that the mineral particles are forming and growing faster when nano-carbonated hydroxyapatite is added. This display that the modified MTA is more biologically active and advisable at encouraging mineral development.

Elemental analysis using energy-dispersive X-ray spectroscopy before and after PBS immersion

The original MTA before soaking had a lot of calcium—about 35.91% by weight—and contained significant amounts of silicon (18.28%), oxygen (23.99%), carbon at 8.97%, along with smaller amounts of bismuth (9.96%) and aluminum (2.89%). Phosphorus was not noticed at this stage. However, after 21 days immersion in PBS, clear changes in elemental composition. Phosphorus (P) came in at 13.60% by weight, while calcium (Ca) dipped a bit to 33.87%. This offered a Ca/P ratio of 2.49, pointing to

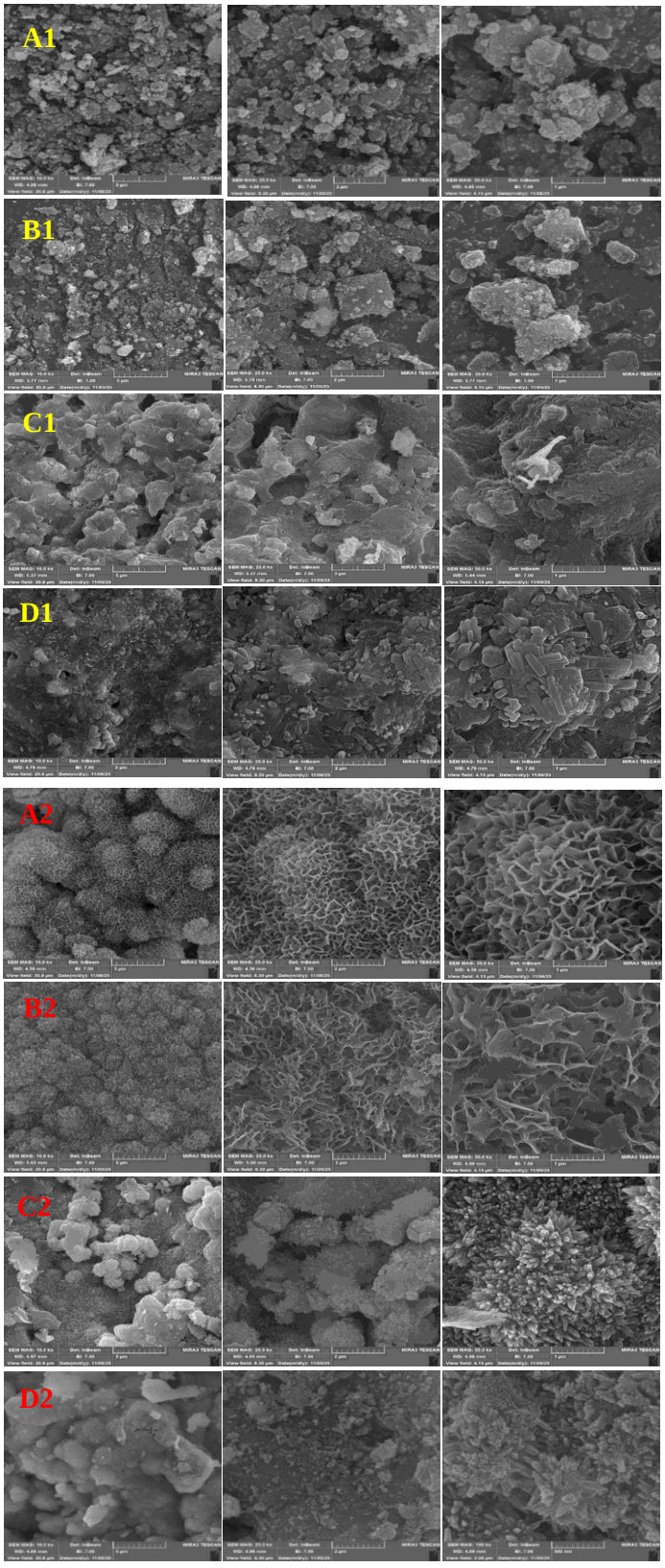

Figure 1. FESEM images illustrating the surface morphology of the cement before (1) and after (2) immersion in PBS. (A) Control group; (B) 2 wt%; (C) 3 wt; and (D) 4 wt% nCHAp experimental groups.

the formation of a calcium phosphate phase, possibly hydroxyapatite. Meanwhile, silicon (Si) and aluminum (Al) both showed a noticeable dropping to 6.91% and 0.89%, respectively. Bismuth content falling to 8.89% while carbon increased slightly to 9.89%, as shown in Table 1. and Figure 2. In contrast, the elemental constitution of modified MTA is shown in Tables 2, 3, 4 and Figure 2. Phosphorus levels increased noticeably after immersion, with higher nCHA content, while Ca showed a slight reduction, resultant in a Ca/P ratio close to that of mature hydroxyapatite. This point to the formation of a stable and well-balanced calcium phosphate layer and reflects improved bioactivity compared to the unmodified group.

Statistical analysis was performed using ANOVA/Tukey tests ($\alpha = 0.05$) (Table 5), the mean Ca/P ratios after 21 days revealed a significant difference among the control and the experimental groups. On the other hand, the groups that were modified with 2%, 3%, and 4% nCHAp showed much lower ratios—1.80, 1.76, and 1.70, respectively. The control group possess a higher Ca/P ratio (2.49, $P < 0.05$), whereas the groups modified with 2%, 3%, and 4% nCHAp showed significantly lower values of 1.80, 1.760, and 1.70, respectively. Although the differences among the modified groups were not statistically significant ($P > 0.05$), all had significantly lower Ca/P ratios than the control. These findings suggest that the addition of nCHAp modulates the apatite chemistry, upgrade the fabrication of a calcium-deficient or carbonated apatite phase, which more closely mimics natural biological apatite. Calcium and phosphorus were the dominant elements at all concentrations, confirming calcium phosphate formation. As nCHAp increased, phosphorus content rose. Also, Ca slightly increased from 35.87% at (2%), 35.81 % at 3%, to 35.72 % at 4%, leading to a progressive reduction in the Ca/P ratio from 1.80 (2%) to 1.70 (4%), toward the hydroxyapatite stoichiometric value, indicating improved bioactivity. Silicon and aluminum contents decreased with higher nCHAp, Whereas C and O showed slight increases from 11.63 % to 12.61 % and from 25.00% to 26.03% respectively, consistent with carbonated apatite deposition. Bismuth levels remained stable, reflecting retention of the radiopacifier.

Table 1. EDX spectroscopy for MTA before and after soaking in PBS

Elements	Mean ± SD	
	Weight% before immersion	**Weight% after 21 days in PBS**
Ca	35.91±0.57	33.87 ± 0.47
P	—	0.80 ± 13.60
Ca/P Ratio	**—**	**2.49**
Si	18.28 ± 0.21	6.91 ± 0.08 Decreased
O	23.99 ± 0.13	25.95 ± 0.29
C	8.97 ± 0.05	9.89 ± 0.17 Increased
Bi	9.96 ± 0.22	8.89 ± 0.18
Al	2.89 ± 0.04	0.89 ± 0.03 Decreased

PBS=phosphate-buffered saline, SD = Standard deviation.

Table 2. EDX spectroscopy for MTA modified with 2% nCHAp before and after soaking in PBS

Elements	Mean ± SD	
	Weight % before immersion	**Weight % after 21 days in PBS**
Ca	36.03 ± 0.31	35.87 ± 0.16
P	5.09 ± 0.24	19.85 ± 0.13
Ca/P Ratio	**—**	**1. 80**
Si	15.89 ± 0.05	3.13 ± 0.19 Decreased
O	24.29 ± 0.22	25.00 ± 0.24
C	9.00 ± 0.13	11.63 ± 0.18 Increased
Bi	7.67 ± 0.13	4.00 ± 0.27
Al	2.03 ± 0.15	0.52 ± 0.10 Decreased

PBS=phosphate-buffered saline, SD = Standard deviation.

Table 3. EDX spectroscopy for MTA modified with 3% nCHAp before and after soaking in PBS

Elements	Mean ± SD	
	Weight % before immersion	**Weight % after 21 days in PBS**
Ca	36.45 ± 0.12	35.81 ± 0.14
P	5.89 ± 0.06	20.31 ± 0.17
Ca/P Ratio	**—**	**1. 76**
Si	13.87 ± 0.10	1.06 ± 0.03 Decreased
O	24.96 ± 0.02	26.01 ± 0.21
C	9.87 ± 0.46	12.55 ± 0.34 Increased
Bi	6.98 ± 0.06	4.02 ± 0.17
Al	1.98 ± 0.58	0.24 ± 0.06 Decreased

PBS=phosphate-buffered saline, SD = Standard deviation.

Table 4. EDX spectroscopy for MTA modified with 4% nCHAp before and after soaking in PBS

Elements	Mean ± SD	
	Weight % before immersion	**Weight % after 21 days in PBS**
Ca	36.89 ± 0.06	35.72 ± 0.26
P	8.42 ± 0.23	21.01 ± 0.02
Ca/P Ratio	**—**	**1. 70**
Si	11.31± 0.14	0.4 ± 0.16 Decreased
O	25.0 ± 0.06	26.03 ± 0.03
C	10.2 ± 0.13	12.61 ± 0.18 Increased
Bi	6.68 ± 0.20	4.02 ± 0.10
Al	1.50 ± 0.24	0.21 ± 0.06 Decreased

PBS=phosphate-buffered saline, SD = Standard deviation.

Table 5. Mean and standard deviation values of the calculated Ca/P ratios at 21 days for control and modified MTA group.

Groups	Ca/P Ratio (Mean ± SD)
Control	2.49 ± 0.138^{B}
2%	1.80 ± 0.064^{A}
3%	1.76 ± 0.167^{A}
4%	1.70 ± 0.089^{A}

Superscript different letters (A, B) denote statistically significant differences ($P < 0.05$).

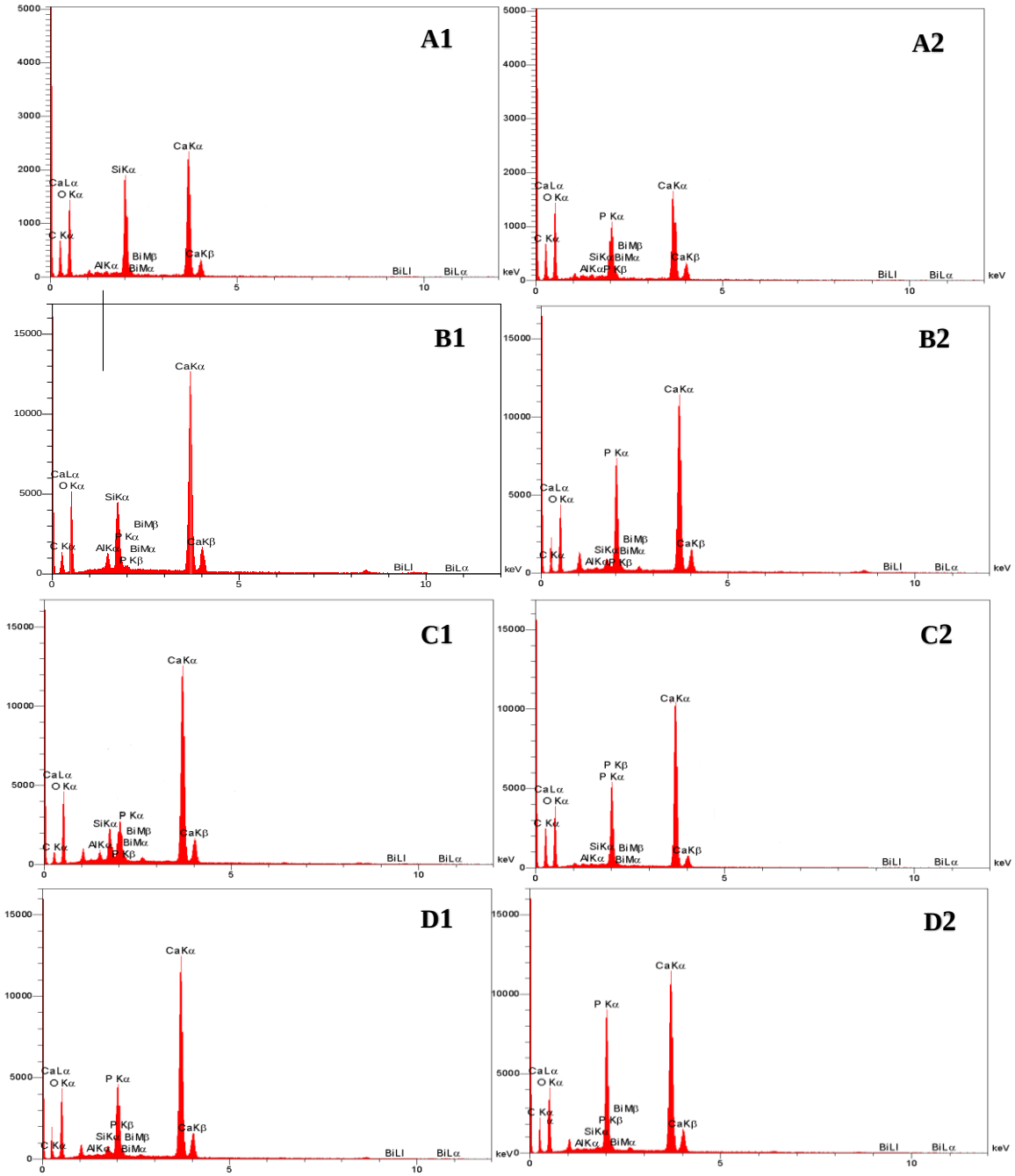

Figure 2. EDX spectra before immersion in PBS (1) and after 21 days of immersion (2), elaborate alteration in elemental composition. Control group (A); 2 wt% (B); 3 wt% (C); and 4 wt% nCHAp (D).

Crystalline phase evolution before and after PBS immersion

The XRD analysis prior to PBS immersion in both unmodified and modified MTA groups (Figure 3 A1, B1, C1 and D1) shows a amorphous profile with well-defined crystalline peaks. Reflections near 18.16°, 28.72°, 34.19°, 36.80°, 54.47° and 64.43° correspond to $Ca(OH)_2$ (ICDD 01-076-0570), indicating that portlandite forms a major hydrated phase. Peaks at 25.02°, 26.11°, 28.66°, 28.86°, 29.51°, 30.10°, 31.53°, 32.69°, 33.91° and 35.02° matches Ca_3SiO_5 (C_3S) (ICDD 00-014-0693) and 26.36°, 28.08°, 31.77°, 32.75°, 34.71°, 45.69°, 50.58°, 51.65°, 53.24° and 54.26° for Ca_2SiO_4 (C_2S) (ICDD 00-024-0037), pointing to unreacted calcium silicates still present in the material. Additional features at 28.34°, 32.84°, 40.51° ,47.12°, 50.17°, 53.09° and 58.63° align with Bi_2O_3 phase (ICDD 01-076-2478). Weak peaks near 30.99°, 32.44° and 44.974° fit $CaCO_3$ (ICDD 00-051-1524) and indicate mild carbonation. No calcium phosphate peaks were observed in the unmodified group, consistent with the absence of phosphorus in EDX analysis. In contrast, the modified group exhibited distinct peaks around 18.29°, 25.57 26.26°, 27.68°, 28.91°, 31.56°, 39.14°, 47.04°—also coincide with calcium phosphate hydrate, $Ca_2(P_4O_{12})\cdot 4H_2O$ (ICDD 00-041-0483). After immersion of MTA (Figure. 3 (A2, B2, C2 and D2)), a relative decrease in the intensity of

the original cementitious peaks was observed, accompanied by an increase in the peak intensity within the 25–35° 2θ range. This indicates ongoing hydration and the formation of calcium-phosphate/apatite-like precipitates on the material's surface, consistent with the well-documented bioactivity of MTA. The broad background between ~10–35° 2θ is still present calcium silicate hydrate (CSH), but there is a slight increase in the intensity of the peaks within this region, appearing near its midpoint. The peaks previously attributed to C_3S/C_2S and Bi_2O_3 remain detectable, although some of them have become relatively less intense compared with the newly enhanced peaks in the 25–35° range. Thus, XRD pattern exhibited substantial changes indicative of mineral phase transformation of unmodified MTA. Notably, new diffraction peaks emerged at 25.87, 31.74, 32.86, 34.04, 39.17, 46.34 which are characteristic of hydroxyapatite ($Ca_{10}(PO_4)_6(OH)_2$), (ICDD 01-072-1243). Some of unreacted calcium phosphate ($Ca_3(PO_4)_2$) characteristic peaks appear at (θ)= 28.26°, 31.75°, 32.45° and 39.46° (ICDD 01-070-0364). The development of these specific peaks supports the precipitation of a calcium phosphate layer, consistent with the EDX observation of a phosphorus content of 13.60 wt% and a Ca/P atomic ratio of 2.49. The relatively high Ca/P ratio suggests the presence of calcium-rich phosphate phases, potentially amorphous calcium phosphate (ACP), but the phase may not yet resemble stoichiometric or mature hydroxyapatite (Ca/P=1.67). Concurrently, modified MTA showed a relative enhancement in the diffraction peaks associated with ($Ca_3(PO_4)_2$) was observed. Specifically, reflections at 2θ 32.08°, 32.45°, 32.75°, 34.214°, 39.46°, 39.66° and 40.58° (ICDD 01-070-0364) increased in intensity especially with 3% nCHA, indicative of ongoing surface mineralization. A new and intensified peaks emerged at 2θ= 25.8°, 28.7°, 31.8°, 33.9°, 39.9°, and 46.7° (ICDD 12-0529), which are representative of carbonated hydroxyapatite (CHA). These findings suggest mineral deposition on the cement surface in response to phosphate. Peaks observed at 25.02°, 29.51°, 31.53°, 32.69° and 33.91° matches C_3S (ICDD 00-014-0693) and 28.08°, 31.77°, 32.75°, 49.29°, 53.24°, 54.26° for C_2S (ICDD 00-024-0037), respectively, were either diminished after immersion and other disappear. A moderate reduction in peaks at 18.16°, 28.72°, 34.19°, 54.47° and 64.43° (ICDD 01-076-0570) was noted, related to portlandite ($Ca(OH)_2$), due to its consumption during apatite precipitation by exchange with phosphate ions. Likewise, peaks at 32.84°, 40.51° ,47.12° and 53.09° (ICDD 01-076-2478) related to (Bi_2O_3), a radiopacifier, showing a slight decrease in relative intensity. Peaks attributable to aluminum-containing phases were below detection limits, in harmony with EDX data that display a significant drop in (Al) content post-immersion. Moreover, peaks at 30.89°, 36.05°,46.84° (ICDD 01-086-2341) connected with ($CaCO_3$), display slight increases, orienting with the rise in C content noticed in elemental analysis. Pure MTA illustrations its typical hydrated pattern. Nonetheless once nCHA added, broad, amorphous hump shrinks, portlandite peaks fade slightly, and those apatite peaks around 26° and between 31–33° become greatly sharper. This shift occurs regularly as nCHA increases from 2% to 3%, distinct peaks showing that the mineral deposits are becoming very crystalline. In 4%, apatite appears more partly carbonated, resultant the reflection broader and less defined sharp.

DISCUSSION

Calcium silicate–based cements promote apatite formation through ion release and alkaline pH in phosphate-rich fluids, enabling calcium phosphate deposition[16,17]. Bioactivity enhances cellular attachment, differentiation, and mineralization[9]. Furthermore, occlusion of dentinal tubules and meliorates sealing [18]. FESEM investigation after immersion revealed that calcium phosphate mineralization on MTA and modified MTA depended on their composition. Unmodified surfaces were covered by porous, spherical layer aggregates with a nanosponge-like attributed to (ACP), formed due to Ca^{2+} released from the hydrated calcium silicate parts of the material and local supersaturation in phosphate-rich environments[19]. Plate-like crystallites inform (OCP) as a passing phase preceding apatite, conformable with the ACP→OCP→apatite pathway[20]. Incorporation of 2% nCHA accelerated this transformation, promoting organized lamellar and plate-like apatite structures through heterogeneous nucleation on nCHA surfaces. Raising the nCHA to 3% produced a uniform surface layer of densely packed with needle- and short plate-like, indicating increased nucleation density and continued crystal growth. At 4% nCHA, showed formation of organized apatite layer of rosette-like assemblies of needle and plate crystallites. Together with the broad, low-intensity apatite XRD peaks, these features are characteristic of nanocrystalline, carbonate-substituted hydroxyapatite typical of bone-like mineral[11, 20, 21]. After 21 days in PBS, EDX analysis presented clear differences in minerals between the unmodified and modified MTA. The original MTA didn't have phosphorus at first, but after it soaked, phosphorus started to show up while calcium dropped, signaling that calcium phosphate was creating on the surface—noticeable mark of bioactivity [22]. Elevated Ca/P ratio (2.49) suggests the predominance of amorphous calcium phosphate rather than stoichiometric hydroxyapatite[23]. The reduction in silicon content reflects silicate leaching and silanol formation that favor apatite nucleation, while minor carbon and decreased Bi and Al suggest surface carbonation and elemental redistribution[24, 25]. Elevated Ca think the effects of continued $Ca(OH)_2$ release and dissolution of nCHAp, both contributive to supersaturation and later apatite formation. While decreased (Bi) signal is assigned to occlusion by newly deposited mineral layers, rather than its dissolution[26, 27]. When nCHAp content increase from 2% to 4%, the Ca and P level increase, while Ca/P ratio declining from 1.80 to 1.70, toward the natural ratio of hydroxyapatite points to the formation of more mature apatite. At the same time, silicon content dropped meditates silicate ion leaching or integration into the structure of apatite, connected to enhanced bioactivity and osteogenic stimulation[28]. The increase in (C) content in the modified groups reinforced the formation of CHA, which

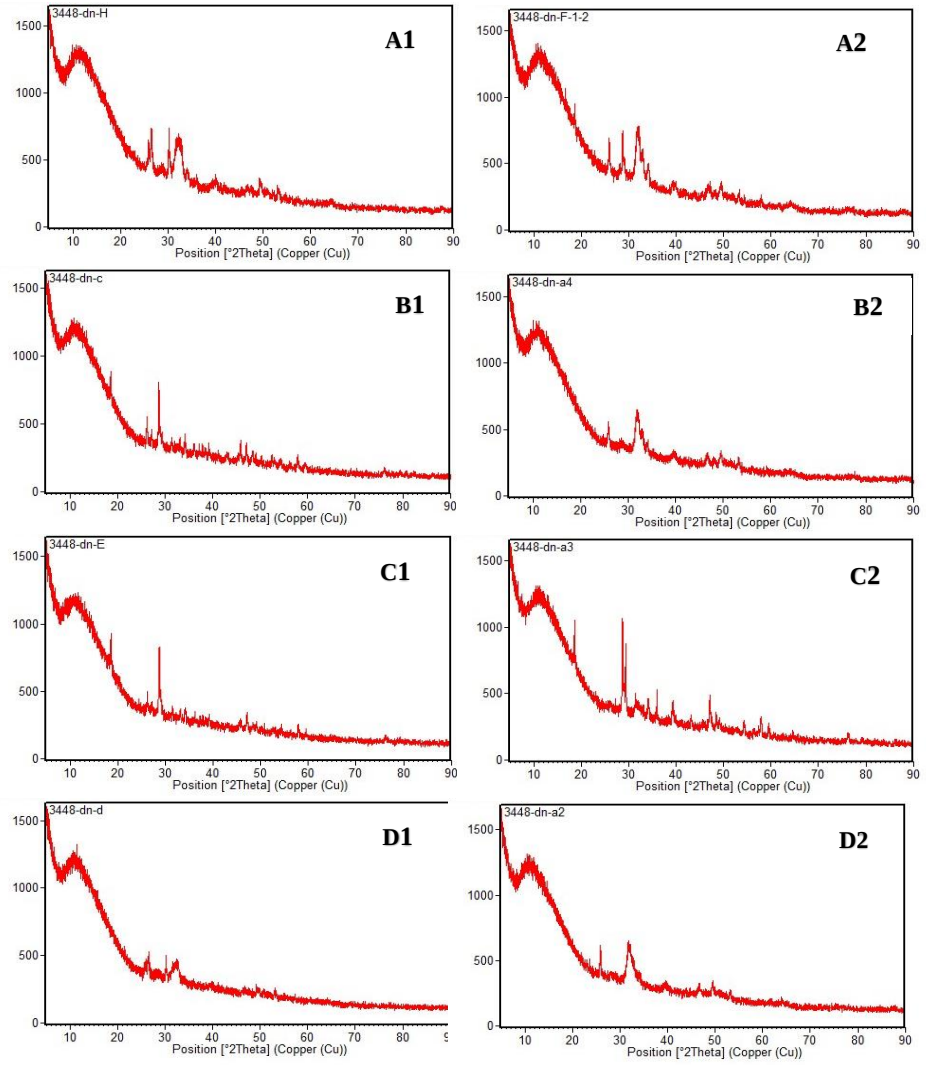

Figure (3): XRD patterns before (1) and after (2) immersion in PBS. Unmodified MTA angelus (A); 2 wt% (B); 3 wt% (C); and 4 wt% (D) integrated nCHAp.

closely mimics bone mineral and exhibit better biologically[29]. On the other hand, lower (Al) levels in the modified groups might be a good action since (Al) concerns to the cell cytotoxicity[30]. The maturity and compatibility of calcium phosphate evaluated by Ca/P ratio. Normally, hydroxyapatite has a Ca/P ratio close to 1.67, whereas biological apatites can vary because of ionic substitutions such as carbonate[31]. Unmodified MTA had upraised Ca/P ratio (2.49), imply there are calcium-rich phases such as portlandite, unreacted calcium silicates, or amorphous calcium phosphate[24]. Quantitative range in 2.0–2.5 can initiate nucleation but also inform supersaturation with calcium oxide phases, which have been coupled to increased oxidative stress, and reduced osteoblast viability[9, 32]. Unlike the pure MTA, the nCHAp-modified type with 2–4% exhibited lower Ca/P ratios, about 1.80 to 1.70, approaching to the ratio in natural carbonated apatite, which imply best phosphate integration and more bone-like mineral formation[26]. Fundamentally, nCHAp do two roles, it supplies phosphate and regarded as a starting point for mineral to form. This shift calcium-rich into well-structured apatite. Also, the carbonate groups speed up the nucleation process[33]. Ca^{2+} and OH^- ions released from hydration of calcium silicates in MTA, make an alkaline, and calcium-rich environment that, in the lack of adequate phosphate or nucleation sites, favour formation of amorphous calcium-rich phases and raised Ca/P ratios, as dictated in the control group[34]. In comparison, nCHAp integration give phosphate, carbonate and supply effective nucleation, promoting the more crystalline, carbonated apatite with Ca/P ratios closer to the native bone [35]. These mineral phases enhance ion balance and chemical stability encouraging cell adhesion, osteoconductivity, compared with unmodified MTA[36]. The higher Ca/P ratio in the control group hints that the mineral phases might be more amorphous or poorly crystalline calcium phosphate, acting as transformation minerals[37]. The strong phosphate peaks in the XRD of the nCHAp samples soaked in PBS display that the surface is mineralizing quicker. It seems to quick build-up of calcium phosphate hydrate layers that then turn into CHA pretty fast[38].

CONCLUSION

Adding nCHAp to MTA enhances early and controlled apatite formation, producing mineral phases and Ca/P ratios closer to natural bone than conventional MTA. This suggests improved mineralization and better

simulation of natural bone formation.

REFERENCES

1. Primozic, J., Hren, M., Mezeg, U., Legat, A. Tribocorrosion Susceptibility and Mechanical Characteristics of As-Received and Long-Term In-Vivo Aged Nickel-Titanium and Stainless-Steel Archwires. Materials. 2022;15: 1427.
2. Vallittu, P.K., Boccaccini, A.R., Hupa, L., Watts, D.C. Bioactive dental materials-Do they exist and what does bioactivity mean? Dental Materials. 2018;34: 693–694.
3. Tiskaya, M., Shahid, S., Gillam, D., Hill, R. The use of bioactive glass (BAG) in dental composites: A critical review. Dental Materials. 2021;37: 296–310.
4. Ghilotti, J., Sanz, J.L., López-García, S., Guerrero-Gironés, J., Pecci-Lloret, M.P., Lozano, A., Llena, C., Rodríguez-Lozano, F.J., Forner, L., Spagnuolo, G. Comparative Surface Morphology, Chemical Composition, and Cytocompatibility of Bio-C Repair, Biodentine, and ProRoot MTA on hDPCs. Materials. 2020;13: 2189.
5. Walsh, R.M., He, J., Schweitzer, J., Opperman, L.A., Woodmansey, K.F. Bioactive endodontic materials for everyday use: A review. Genral Dentistry, 2018;66: 48–51.
6. Schmalz, G., Hickel, R., Price, R.B., & Platt, J.A. Bioactivity of dental restorative materials: FDI policy statement. International dental journal. 2023;73(1): 21-27.
7. Pushpalatha, C., Dhareshwar, V., Sowmya, S.V., Augustine, D., Vinothkumar, T.S., Renugalakshmi, A., .. & Patil, S. Modified mineral trioxide aggregate—A versatile dental material: An insight on applications and newer advancements. Frontiers in bioengineering and biotechnology. 2022;10; 941826.
8. Kunert M., Piwonski I., Hardan L., Bourgi R., Sauro S., Inchingolo F., & Lukomska-Szymanska M. Dentine remineralisation induced by “bioactive” materials through mineral deposition: an in vitro study. Nanomaterials. 2024;14(3): 274.
9. Gandolfi, M.G., Spagnuolo, G., Siboni, F., Procino, A., Rivieccio, V., Pelliccioni, G.A., & Rengo, S. Calcium silicate/calcium phosphate biphasic cements for vital pulp therapy: chemical-physical properties and human pulp cells response. Clinical oral investigations. 2015;19(8): 2075-2089.
10. Okiji T, Yoshiba K. Reparative dentinogenesis induced by mineral trioxide aggregate: a review from the biological and physicochemical points of view. International journal of dentistry. 2009;2009(1):464280.
11. Priyadharshini S.S., Ragavendran C., Sherwood A., Ramya J.R., & Krithikadatta J. Evaluation of mineral induction ability and cytotoxicity of carbonated hydroxyapatite for pulp tissue regeneration: an in vitro study. Restorative Dentistry & Endodontics. 2024;49(4): e40.
12. International Organization for Standardization. Implant for surgery-in vitro evaluation for apatite-forming ability of implant materials. In: International Standard ISO 23317. 3rd ed. Geneva, Switzerland: ISO; 2014. p. 1-12.
13. Al-Askary RA, Al-Ashou WM, & Al-Jubori SH. In Vitro Apatite-Forming Ability of Different Root Canal Sealers (A Comparative Study). Journal of International Society of Preventive and Community Dentistry. 2025;15(2):173-183.
14. Hoikkala NJ, Wang X, Hupa L, Smått JH, Peltonen J, Vallittu PK. Dissolution and mineralization characterization of bioactive glass ceramic containing endodontic sealer GuttaFlow Bioseal. Dental Materials Journal. 2018;37:988-94.
15. Prüllage RK, Urban K, Schäfer E, Dammaschke T. Material properties of a tricalcium silicate-containing, a mineral trioxide aggregate-containing, and an epoxy resin-based root canal sealer. Journal of endodontics. 2016;42:1784-8.
16. Al-sherbiny IM, Farid MH, Abu-seida AM, Motawea IT, Bastawy HA. Chemico-physical and mechanical evaluation of three calcium silicate-based pulp capping materials. Saudi Dental Journal. 2021;33: 207-14.
17. Abo El-Mal EO, Abu-Seida AM, El Ashry SH. A com¬parative study of the physicochemical properties of hesperidin, MTA-Angelus and calcium hydroxide as pulp capping materials. Saudi Dental Journal. 2019; 31: 219- 27.
18. Reyes-Carmona JF, Felippe MS and Felippe WT. Biomineralization ability and interaction of mineral trioxide aggregate and white portland cement with dentin in a phosphate-containing fluid. Journal of endodontics. 2009; 35: 731–736.
19. Camilleri J. Hydration mechanisms of mineral trioxide aggregate. International endodontic journal. 2007;40(6):462-470.
20. Rey C, Combes C, Drouet C, Glimcher MJ. Bone mineral: update on chemical composition and structure. Osteoporosis international. 2009;20(6):1013-21.
21. Shepherd J.H., Best S.M., & Cameron R.E. Carbonate substitution in apatite formed in simulated body fluid. Biomaterials. 2012;33:1089–1099.
22. Primus C.M., Tay F.R. & Niu L.N. Bioactive tri/dicalcium silicate cements for treatment of pulpal and periapical tissues. Acta Biomaterialia. 2019;96: 35-54.
23. Hou X., Zhang L., Zhou Z., Luo X., Wang T., Zhao X., ... & Zheng L. Calcium phosphate-based biomaterials for bone repair. Journal of functional biomaterials. 2022;13(4):187.
24. Niu L.N., Jiao K., Wang T.D., Zhang W., Camilleri J., Bergeron B.E,..& Tay F.R. A review of the bioactivity of hydraulic calcium silicate cements. Journal of dentistry. 2014;42(5):517-533.
25. Liu X, Feng P, Cai Y, Yu X, Yu C, Ran Q. Carbonation behavior of calcium silicate hydrate (CSH): Its potential for CO2 capture. Chemical Engineering Journal. 2022;431:134243.
26. Yotsova R. & Peev S. Biological properties and medical applications of carbonate apatite: a systematic review. Pharmaceutics. 2024;16(2); 291.
27. Dehkord, E.S., De Carvalho, B., Ernst, M., Albert, A., Lambert F. & Geris L. Influence of physicochemical characteristics of calcium phosphate-based biomaterials in cranio-maxillofacial bone regeneration. A systematic literature review and meta-analysis of preclinical models. Materials Today Bio. 2024; 101100.
28. Kokubo T. & Takadama H. How useful is SBF in predicting in vivo bone bioactivity? Biomaterials, 2006; 27(15): 2907-2915.
29. Germaini M.M., Detsch R., Grünewald A., Magnaudeix A., Lalloue F., Boccaccini A.R. & Champion E. Osteoblast and osteoclast responses to A/B type carbonate-substituted hydroxyapatite ceramics for bone regeneration. Biomedical Materials. 2017;12(3):035008.
30. Saghiri M. A., Gutmann J. L., Orangi J., Asatourian, A. & Sheibani N. Radiopacifier particle size impacts the physical properties of tricalcium silicate–based cements. Journal of endodontics. 2015;41(2); 225-230.
31. Jamilludin M.A., Dinatha I.K.H., Supii A.I., Partini, J., Kusindarta D.L. & Yusuf Y. Functionalized cellulose nanofibrils in carbonate-substituted hydroxyapatite nanorod-based scaffold from long-spined sea urchin (Diadema setosum) shells reinforced with polyvinyl alcohol for alveolar bone tissue engineering. RSC advances. 2023;13(46): 32444-32456.
32. Lai Y., Gao F.F., Ge R.T., Liu R., Ma S. & Liu X. Metal ions overloading and cell death. Cell Biology and Toxicology, 2024;40(1):72.
33. Lu T., Yan S., Shi H. & Ye J. Synthesis, characterization, in vitro cytological responses, and in vivo bone regeneration effects of low-crystalline nanocarbonated hydroxyapatite. ACS Biomaterials Science & Engineering. 2023;9(2):918-931.
34. Elbatanony M.M., Safwat E.M., El-Sherif S. & Hassan M.L. Resin-based dental pulp capping restoration enclosing silica and portlandite nanoparticles from natural resources. Scientific Reports. 2024; 14(1):16554.
35. Wang Z., Shimabukuro M., Kishida R., Yokoi T. & Kawashita M. Effects of pH on the microarchitecture of carbonate apatite granules fabricated through a dissolution–precipitation reaction. Frontiers in Bioengineering and Biotechnology. 2024;12:1396275.
36. Habiburrohman M.R., Jamilludin M.A., Cahyati N., Herdianto N., & Yusuf Y. Fabrication and in vitro cytocompatibility evaluation of porous bone scaffold based on cuttlefish bone-derived nano-carbonated hydroxyapatite reinforced with polyethylene oxide/chitosan fibrous structure. RSC advances. 2025;15(7):5135-5150.
37. Ranjkesh B., Chevallier J., Salehi H., Cuisinier F., Isidor F. & Løvschall H. Apatite precipitation on a novel fast-setting calcium silicate cement containing fluoride. Acta Biomaterialia Odontologica Scandinavica. (2016);2(1): 68-78.
38. Abu-Zeid S.T., Saif R.E., Mostafa H.A. & Edrees H. Y. Characterization and crystallinity of two bioactive sealers: Qualitative and quantitative analysis. Applied Sciences. 2024;14(3):1285.